https://doi.org/10.26682/sjuod.2023.26.2.67

Journal of University of Duhok., Vol. 26, No.2 (Pure and Engineering Sciences), Pp 754 - 771, 2023
(Special Issue)

MOVING DIPOLE LOCALIZATION USING LINEAR LEAST SQUARE ESTIMATION: A REVIEW

IMAD ABDULKAREEM DAWOD[*], THOMAS SCHANZE[**] and SALIH MUSTAFA S. ATROSHEY[*]
[*] Dept. of Biomedical Engineering, University of Duhok, Kurdistan Region -Iraq
[**]IBMT, Dept. Life Science Engineering, THM- Germany

(Accepted for Publication: November 27, 2023)

ABSTRACT

In this review study we will shed some light on the equivalent source generators in electrocardiography and specially the moving dipole (MVD) and the characteristics of biomedical models used with this type of equivalent source generator. The mathematical derivation of the equations used in localizing this MVD is presented with the clarification of the reasons of inaccuracies due to; non-uniqueness, instability (ill-posedness) of the solution, and how a linear least square estimator method may improve the uniqueness of the solution. In addition, its experimental check in different inhomogeneity situations is also stated, the effect of blood mass on the moment and direction of the dipole throughout the ECG course is discussed too. The contribution and/or the progress of different groups of researchers in the clinical validation of MVD is concisely mentioned, furthermore some modern applications of the MVD are also presented.

KEYWORDS*:* Electrodes number and interspacing, Forward and inverse problem, Heart models, Least squares estimation, and Moving dipole

1. INTRODUCTION

In biomedical engineering, models can predict the function of different systems and organs of the human body (Malmivuo, J., & Plonsey, 1995). Models with hypothesis describe and dictate the inter relationship between the different variables of systems that are difficult to be obtained in practical experiments. Laws of electrical or mechanical engineering and chemistry are used to represent those relationships, and the electric field effect (e.g., the forward problem and the inverse problem) and mathematical analysis (e.g., least squares analysis) are used to verify the hypothesis or workout the solution to the invers problem. In this review study, an electrical source, the heart model in the form of a moving dipole(MVD)(Gabor & Nelson, 1954), is used to describe the complete heart function(Geselowitz, 1964). Its non-invasive(i.e., surface body) localization which was clinically validated by (Ideker et al., 1975), is compared with other sources localization method used by different researchers in this field (indicative of heart illnesses (Savard et al., 1985)) and some recent applications of the MVD(Armoundas, Feldman, Mukkamala, He, et al., 2003; Bystricky, 2012, 2018; Selvester et al., 2010; Starc & Swenne, 2017).

2. MODELS

The biomedical heart model is based on the electrical engineering concept of the distributed volume source and volume conductor. Inductors are non-existent in the human body as for resistance, batteries(source), and capacitances they are distributed too. Capacitance is due to cell membrane and affect the conduction velocity. In electrocardiography the source is within the heart and the conductor is the whole body (Malmivuo, J., & Plonsey, 1995). Within the frequency range of 0.1-10 kHz(which is the spectral range of the physiological heart activity) the human body can be regarded as purely resistive(Kay, C. F. Schwan, 1956).

Before going any further in the electrocardiographic heart model source and conductor types, it should be made clear that certain heart volume sources are associated with certain volume conductors and the association is based on certain preconditions(assumptions); these preconditions include that volume conductors are all linear and isotropic(homogeneity assumption) especially in the field of body surface methods which often noninvasive(Gulrajani, 1998). The term “isotropic” here means that the conductivity has the same value when measured in different directions. Volume conductor is considered

isotropic for the different regions of the torso as **(1)** Heart 1.6 Ωm, lung 4 Ωm, and blood regions 20 Ωm, or as semi-isotropic if the muscles of the overlying part are considered.
(2) Lung is uniform 1 Ωm, and heart and the surface muscle 10 Ωm(Rush, 1971).

The body surface potentials (forward problem) can be measured by two methods; surface method and volume method. If the voltage is measured on the body surface, or the potentials of the epicardium(Lv et al., 2020; Svehlikova et al., 2018); it is called surface method and both of them can be solved by integral equations. If on the other hand volume method is used which is more complex than surface method(Houari et al., 2018; Nakane et al., 2019; Nakano et al., 2021); the torso is divided into small elements and either finite elements or finite difference method is used in addition more potentials are often used and those potentials are described in terms of its neighboring point.

As for sources which represents ions that move between the intracellular and extracellular domain through the cell membrane, and as this membrane is very small those ion charges can be considered as dipoles(Geselowitz, 1964; Macfarlane, P. W., Van Oosterom, A., Pahlm, O., Kligfield, P., Janse, M., & Camm, 2010). Those charges can constitute an infinitesimal current. The different types of sources used in electrocardiography are

- Monopole.
- Dipole and moving dipole.
- Multiple dipoles.
- Multipole.
- Etc.

Each of these models has different variables that describe its behavior and relate it to a specific area of the heart; variables are magnitude, location, and orientation. Anyway, it should be emphasized here that in this paper we deal only with moving dipole(MVD), which generally have variable size and orientation and location

2-1. DIPOLE

An electric dipole consists of two equally sized neighboring particles of opposite charges. The equation of the dipole potential can be derived using Coulomb's Law (conservation of charge) and under the assumption that the ratio between the separation of the two different charges(**d**) and the distance to a point in space(**r**) is sufficiently large, e.g., larger than one tenth. In bioelectromagnetsim **r** >> **d** holds (Plonsey, R., & Barr, 2007) (shown in Figure1: (A)and (B) below) or stating it in another way the strict definition requires with **p**=q***d** in the limit being finite(where **p** is dipole moment, and -q and q are negative and positive charge and **d** is the displacement vector pointing from the negative charge to the positive charge).

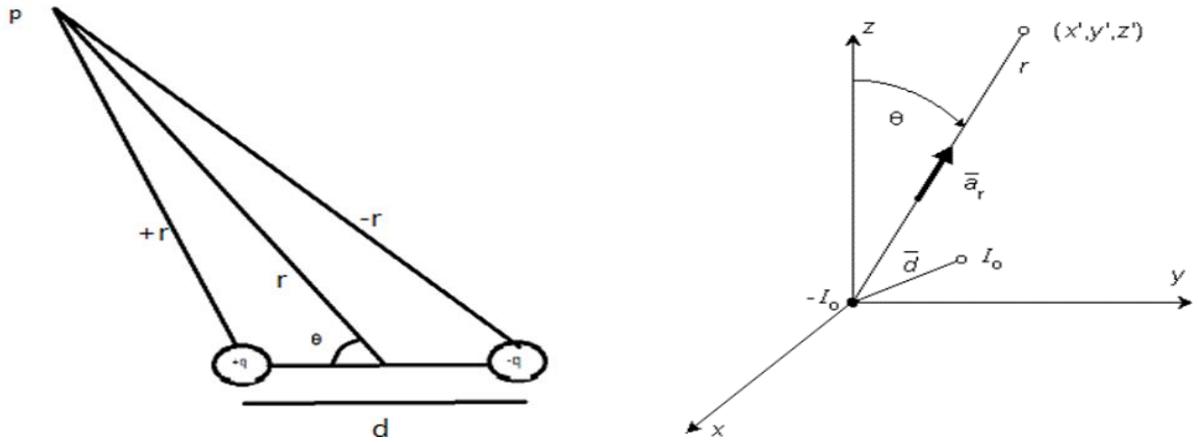

(A) (B)

Fig.(1):- Simplified dipole model. (A) Two opposite charges position relative to point P in space(or in a field) (B)Source and sink(monopoles) in 3D coordinate(Malmivuo, J., & Plonsey, 1995).

The potential equation for the simplified dipole Equation **Error! Reference source not found.**

$$\varphi = \frac{kP\cos\theta}{r^2} \qquad (1)$$

Where φ is dipole potential due to a point in space(in field), k is Columb's constant the value of which is 8.99×10^9 Nm2/ columb2, p is the dipole strength, r distance between the point where the potential is measured and the dipole coordinates (Samann et al., 2019).

3. ELECTRIC FIELD EFFECT AND MATHEMATICAL ANALYSIS

3-1. Forward and Inverse Problem

The forward problem is defined as calculating or measuring the electric field(on surface body voltages) of the equivalent source (in our case is the MVD), i.e., measuring and interpretation of the body surface voltages is straight forward. However, if the heart source and the volume conductor properties are known, then the computing of the forward problem is easy. But real signals can be corrupted by noise to some degree by the geometry which may result from geometric model, errors due to numerical solution, errors in different region in conductivities, and also due to the positions of the electrodes. Thus, a comparison between simulated and measured data is often elaborate.

The inverse problem on the other hand is defined as calculating the source position having the field measurements (voltages including electrode's positions) knowledge about the volume conductor as shown in the Figure2, the solution to the inverse problem is generally not unique. This also can be a result of the volume conductor approximation and additional voltage sources, which may be represented by different Thevenin's or Norton's equivalent circuits(McFee & Baule, 2008).

The ECG inverse problem is often unstable and sensitive to small changes, especially noise that can produce large solution errors (Nguyen & Schanze, 2017; Samann et al., 2019). However, the solution is also sensitive to changes in geometry or configuration of the model (Nguyen & Schanze, 2017). The sensitivity or instability of the inverse problem is often termed ill posed (Kabanikhin, 2008).

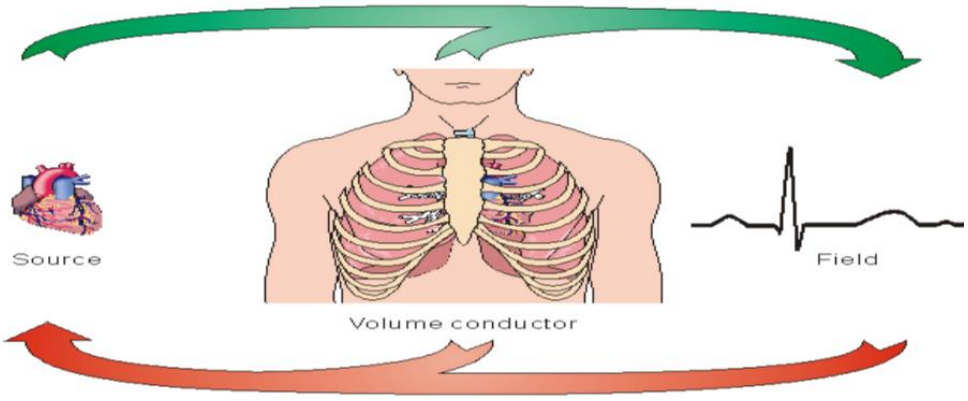

Fig.(2):- The Forward Problem (green curved arrow) and the Inverse Problem (red curved arrow) (Malmivuo, J., & Plonsey, 1995).

3.2. Least Square Method

An optimization method that uses the minimization of the sum of square residuals, minimizes the difference between two sets of values like calculated and experimentally measured ones. The unknowns of Equation**Error! Reference source not found.** can be computed by least square method given potentials recorded with electrodes of given positions of the body surface. Thus, we have to estimate 4 parameters, i.e., k, p, θ and r. When the orientation of the dipole is not known, then the potential of a dipole located at rd in the origin of a homogeneous medium is given by Equation**Error! Reference source not found.**

$$\varphi(\mathbf{r}) = \frac{\mathbf{e}_r \cdot \mathbf{p}}{4\pi\varepsilon_r\,\varepsilon_0|\mathbf{r}-\mathbf{r}_d|} \qquad (2)$$

where $\mathbf{e}_r$, $\mathbf{p}$, ε_r, ε_0, are unit vector from source to field, p = p*a (a is unit vector in the direction of the displacement), relative

permittivity, permittivity of free space respectively. This means that six parameters of the dipole must be estimated, three for position and three for dipole moment. When six potentials including their recording positions are known, then the estimation of the six parameters is possible(Nguyen & Schanze, 2017; Samann et al., 2019). In case of noisy signals, we need more potentials in order to find the parameters by solving an overdetermined system of equations, e.g., by least squares method.

4. MOVING DIPOLE MVD

4-1. Moving Dipole Localization Mathematical Treatment

The idea of a moving dipole in electrocardiography came first by (Gabor & Nelson, 1954) in their classical paper where they showed mathematically that for a uniform distributed homogeneous conductor the magnitude(strength), orientation, and location of the equivalent current source generator can be estimated from measuring body surface voltages and the shape of the body. They used vector calculus; and employed the resultant of first and second moments of a current source. They obtained a set of three integral equations from first moment Equations**Error! Reference source not found.**, **Error! Reference source not found. Error! Reference source not found.** (to find the strength and direction of the dipole) and another six equations (or rather five as one can be eliminated by addition) from combining the first and second moment equations(to find the location of the dipole) Equations**Error! Reference source not found.Error! Reference source not found.Error! Reference source not found.Error! Reference source not found.Error! Reference source not found.** as shown below

$$M_x = k \iint V\, dz\, dy \quad (3)$$
$$M_y = k \iint V\, dx\, dz \quad (4)$$
$$M_z = k \iint V\, dx\, dy \quad (5)$$
$$M_x X - M_y Y = k\ [\iint x\, V\, dz\, dy - \iint y\, V\, dx\, dx\ ] \quad (6)$$
$$M_y Y - M_z Z = k\ [\iint y\, V\, dz\, dx - \iint z\, V\, dx\, dy\ ] \quad (7)$$
$$M_x X - M_z Z = k\ [\iint x\, V\, dz\, dy - \iint z\, V\, dx\, dy\ ] \quad (8)$$
$$M_y X - M_x Z = k\ [\iint x\, V\, dz\, dy - \iint x\, V\, dz\, dx\ ] \quad (9)$$
$$M_z X - M_y Z = k\ [\iint z\, V\, dz\, dy - \iint y\, V\, dx\, dy\ ] \quad (10)$$
$$M_x X - M_z Z = k\ [\iint x\, V\, dx\, dy - \iint z\, V\, dz\, dy\ ] \quad (11)$$

1ST moment equations

2nd moment equations

where k, V, $M_{x,y,z}$, $X, Y, and\ Z$,are uniform isotropic conductivity, potential measured on the surface of body, moment in the x, y, and z coordinates direction, and the location of the dipole in x, y, and z coordinates respectively Equation**Error! Reference source not found.Error! Reference source not found.** can be added and yield Equation**Error! Reference source not found.** and we end up with five equations for the second moment instead of 6 equations. They proposed two ways to solve them; one by solving three integral equations (to obtain the location i.e., X, Y, and Z coordinates of the source) leaving the other two redundant equations for checking the results(more elaborate details can found in (Gabor & Nelson, 1954, Nelson et al., 1975)), and the other way was by using least square method. They also extended this idea of moving dipole (resultant of set of source and current sinks) to finding the location of more than on dipole by employing the third moment of the dipole source in which they derived a set of nine equations containing the first moments and by cyclic interchange and elimination end up with seven equations. It should be mentioned here there is another mathematical way for calculation or localization of MVD equivalent source generators“ the multipole series expansion” which can also be evaluated from the voltage body surface but with geometry of the body not the shape of the body (Geselowitz, 1964), this method too uses the least square estimation. This method was investigated by Geselowitz and is used to explain the abnormal behavior of the heart (Geselowitz, 1965).

4-2. Moving Dipole Localization Experimental Check

This theory was tackled experimentally(Nelson et al., 1975) by using a tank resembling the shape of human thorax filled with an electrolytic solution and by placing a dipole in the heart area and measuring the voltages distribution around the thorax as shown in the Figure3. The agreement between measured results and the calculated ones were for orientation angle 1° and for location of dipole 0.5cm. Taking in consideration the lungs conductivity (inhomogeneity) and using the ratio of one quarter to its surrounding was used and also gave very satisfactory results of 4° for the angle and 0.6 cm for the locations. When assuming the lung is partly an insulator the results for the angle was still satisfactory 4° but for the location it was 6 cm due to the high value of conductivity used which didn't take account for the lower part of the tank used.

The effect of blood mass was also investigated by (Nelson et al., 1972). Due to the fact that QRS diastolic start when the volume of the ventricle is the largest; a change in blood mass quantity (or its resistivity) will contribute to the change in ventricle volume and as result to the ECG and particularly to QRS portion. In experiments conducted on dogs; blood was withdrawn and reinfused and the resistivity of the blood (or the density of the blood) was controlled by controlling the hematocrit. Furthermore, if in a situation where the blood resistivity can be controlled to be equal to that of the heart tissue a homogenous state can be reached and results in more accurate real values. It was shown from a lead system devised by (Nelson, C. V., Gastonguay, P. R., Wilkinson, A. F., & Voukydis, 1971) and used to find the dipole moment and its direction, that the moment vector M of the dipole in normal conditions had three peaks M_1 , M_2 , and M_3 according to their occurrence with respect to QRS. The mean of M_1 during the 29 % and M_2 during 42% (i.e., nearly during the 1^{st} half of the QRS) and M_3 during the 64% (i.e., during the 2^{nd} half of the QRS). The change in the moment vector M_1, M_2 is in the radial direction for the first portion of the QRS while for M_3 is tangential. When blood resistance changed to be equal to the heart tissue resistance (i.e., homogeneity condition) M_1 increased by 3 folds, M_2 increased by 2.5 folds and M_3 decreased nearly by 25%. P wave changed in a manner similar to QRS and directed tangentially as for T wave the results were inconclusive but in general, they increased.

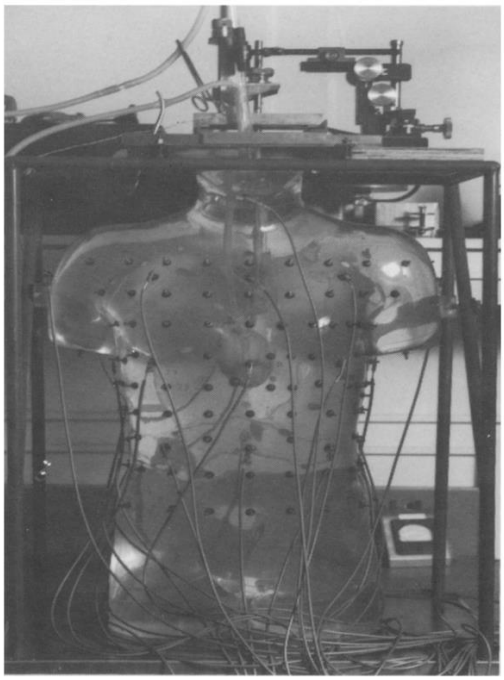

Fig.(3):- Experimental setups of the simulated human thorax model filled with fluid with electrodes laid over thorax surface(Nelson et al., 1975).

4-3. Moving Dipole Localization Clinical Prove

Moving dipole localization(also called dipole ranging) has been tested clinically by a number of researchers by different methods. (Martin Arthur's et al., 1971) used 2800 points on the surface of human torso to describe 1426 triangular element each with three vertices coordinates; and with the help of biplane imaging; (coronal and longitudinal) of the heart silhouette are obtained. The center of gravity of the X-ray was chosen to be the equivalent source location and the position of the moving electrical center(MEC) during the different heart phases was examined. (Brody et al., 1971) used a spherical container made of two identical epoxy hemi-spheres, one of them has adaptable support, the chamber has 20 evenly spaced electrodes installed on its inner surface and its diameter is 6.25 cm shown in Figure4. An isolated beating heart of turtle was immersed in this spherical tank filled with Ringer's solution and from the 20 electrodes that were organized in pairs; 10 signals were obtained and they were used to represent the parameters of dipole (3) and parameters of octupole (7) and solved using the multipole series expansion.

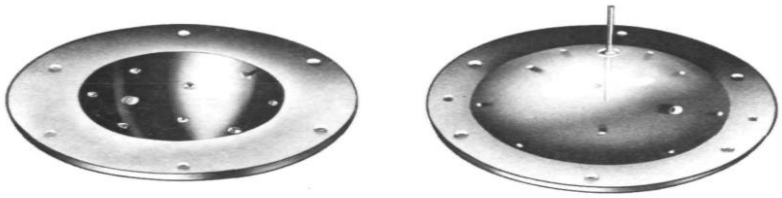

Fig.(4):- Spherical container consisting of upper and lower parts, 20 electrodes fixed from inside; used to study the field effect of the beating heart of a turtle (Brody et al., 1971).

(Brody & Wennemark, 1974) in another setup in which isolated rabbit heart immersed in chamber filled with Krebs-Henseleit solution (KH) and some modification to the chamber used in his previous study of the turtle heart that allow for synchronizing camera photograph taking with start of QRS segment and data acquisition as shown in Figure5. Then this is followed by sectioning the right bundle branch and repeating the same procedure, to make sure that the right bundle branch was cut to the desired depth and width it was stained with Lugol's solution. The signals obtained are resolved into the different source generators of dipole, quadrupole, octupole, and hexadecapolar. The dipole coefficients and their mathematical expression are compared and an iso-potential map over the chamber surface was obtained. From this iso-potential mapping they derived a qualitative directional location estimation. They quantitively find dipole location by using the 20 signals obtained from the chamber's sensor by feeding them to shifting equations and using the least square estimation method. Their conclusion was that eccentricity of the source is not a big problem because with their dipole ranging method 90% accuracy was obtained.

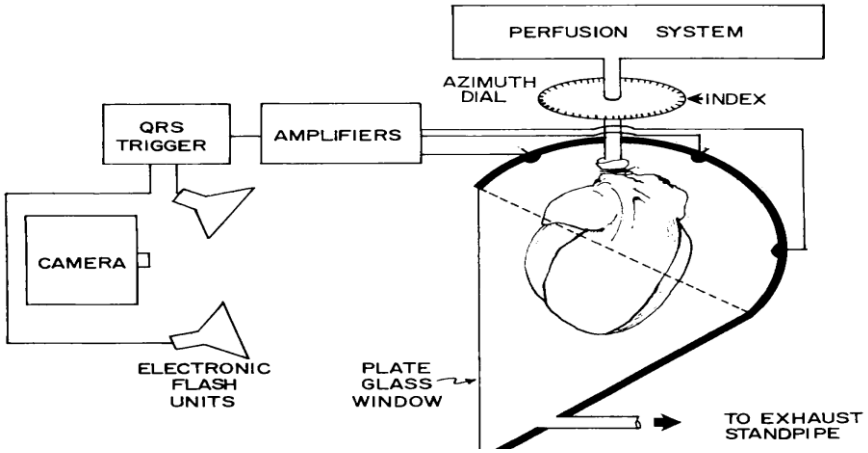

Fig.(5):- Synchronizing photographs triggering and data acquisition integrated in the chamber(Brody & Wennemark, 1974).

(Ideker et al., 1975) in his work tried to enhance the finding of the former work or rather to validate the dipole localization clinically. Using 20 isolated rabbit hearts in two scenarios: one by epicardial cauterizing 14 of them and the other scenario is by ventricular pacing of the remaining 6. This was done in a spherical apparatus similar to the one used in the previous study by (Brody & Wennemark, 1974) with the same number of electrodes (20). In this spherical container a window was introduced to view the cauterization area as shown in Figure6.

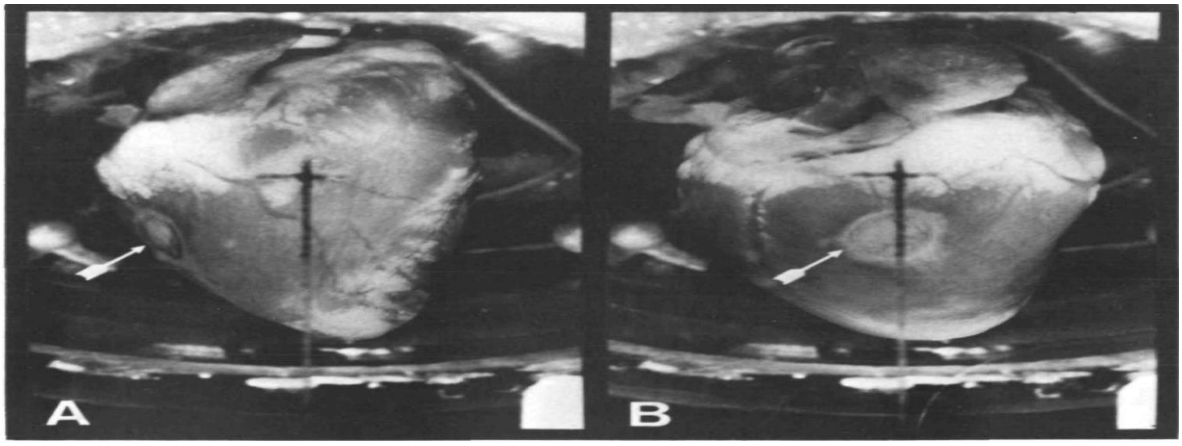

Fig.(6):- Two views of isolated rabbit heart in the chamber showing the cauterized region. White arrow pointing toward(circle shape) cauterized area (Ideker et al., 1975).

For the first 14 specimens two kind of signals are obtained as shown in Figure7. One when the electrode of the chamber touches the cauterized part of specimen (circle shape) and the other when the electrode touches the intact specimen.

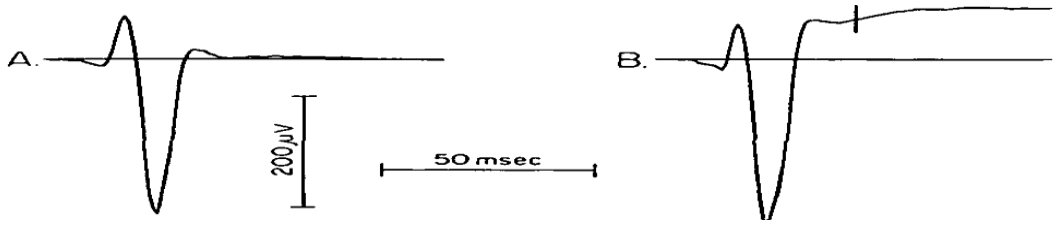

Fig.(7):- Potentials recorded during the QRS complex and the early S-T segment by; A electrodes touching the cauterized specimen part and, B by electrode touching the intact part of the specimen; the early commencement of the S-T segment which is represented by a vertical mark on B indicate the isopotential surface on Figure (8) (Ideker et al., 1975).

Electrode positions relative to the cauterized area of the heart is shown in Figure8, which represents the potential distribution on the surface of the container 7 msec later of the commencement of the S-T segment.

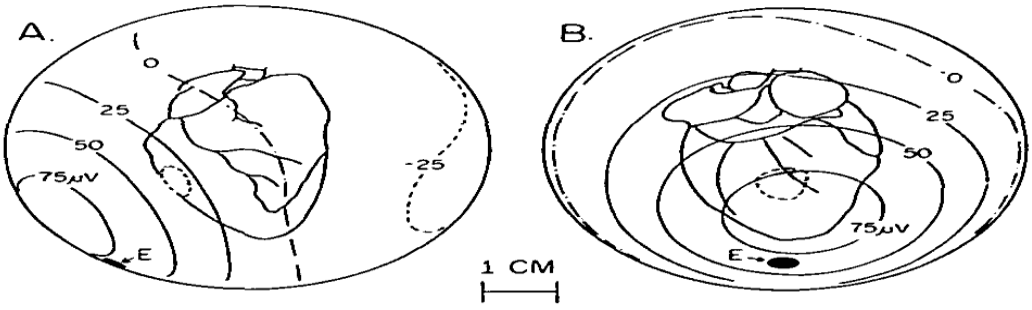

Fig.(8):- Potential distribution on the spherical container; E represent the electrode 18 position and cauterized area are represented by the small dotted circle(Ideker et al., 1975).

It's evident from Figure8, the shape of the potential distribution which has smooth transition from maximum to minimum value, that the behavior is that of a dipole.

The equivalent dipole is found by iterative method using a mathematical procedure described in (Terry et al., 1971) for the two intervals of the heart cycle QRS and ST segments every millisecond. This linear least square optimization method produced the strength, orientation, and location of the dipole using the potentials of the 20 electrodes in the chamber. The distance of the locus of computed equivalent dipole to the center of the cauterized region is shown in Figure9. This distance is less than 1/3 of the radius of the cauterized region taken as average for the 14 specimens.

	MEAN (mm.)	S.D. (mm.)
BURN RADIUS	5.0	1.3
LINE CD	3.2	1.0
LINE CD'	1.7	1.1
LINE D'D	2.0	1.7
ANGLE M_DN_C	13.5°	6.9°

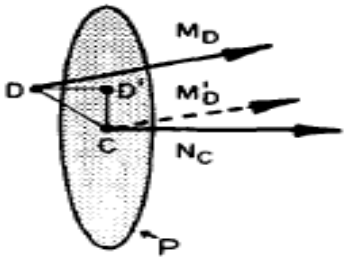

Fig.(9):- Difference between the calculated and cauterized dipole vectors. P is periphery of the cauterized region. DD' , calculated location vector of the cauterized region and its projection on the plane of the cauterized region respectively. M_D , M_D', computed dipole moment and computed dipole moment moved to the center of the cauterized region respectively. N_c is the vertical to the plane of the cauterized region, and the S.D is the standard deviation(Ideker et al., 1975).

From Figure9, it can be seen that inward shift of the dipole from the center of the cauterized region (D'D) is the main cause of the difference between the center of the cauterized region and the calculated dipole.

The root mean square voltages residual is the remaining potentials of 20 potential recording electrodes on the chamber surface after the removal of the portion of the equivalent dipole and it was found from Figure9, to be 11.9%; it represents the non-dipolar portion of the seventh millisecond of the ST segment and because the root mean square of the surface is Pythagorean totality of the dipole and residual effect(Horan et al., 1972), that is mathematically represented as in Equation**Error! Reference source not found.Error! Reference source not found.Error! Reference source not found.Error! Reference source not found.**

$$1 = \sqrt{\left(D_{effct}\right)^2 + \left(R_{effct}\right)^2} \qquad (1)$$

$$D_{effct} = \sqrt{1 + \left(R_{effct}\right)^2} \qquad (13)$$

$$D_{effct} = \sqrt{1 - (0.119)^2} \qquad (14)$$

$$D_{effct} = 0.993 \qquad (15)$$

where D_{effct} is percentage of root mean square of dipole effect and R_{effct} is percentage of root mean square residual effect and this result which is very important result states that the total of root mean square of dipole effect contributes to 99.3% of the total surface potentials.

More accurate findings further consolidated the above results in a study by (Claydon et al., 1992) in which they obtained that the root mean square error between calculated and measured isopotential maps values of a single MVD measured from inside the heart by inserting intercavitary probe (Taccardi et al., 1987) to be 11.5 % .

5. Moving Dipole Localization and Electrodes Number and Configuration

As stated, above, electrodes play an important role in enhancing the localization procedure of the MVD. In a simulation study by (Savard et al., 1982) in which a modified torso model with finite element as the one used by (Horáček, 1971) shown in Figure10. This finite element model was compromised of 19 horizontal section each made of 67 triangles with total of 1216 surface elements form which 326 triangles for the lungs and 264 for blood mass. On each of the surface element the generated potential by a given source is obtained by one solid angle, (Barnard et al., 1967) and (Lynn & Timlake, 1968). The setup, procedure, and mathematical treatment of the study had number of goals the one most relevant to our study is the lead system configuration results.

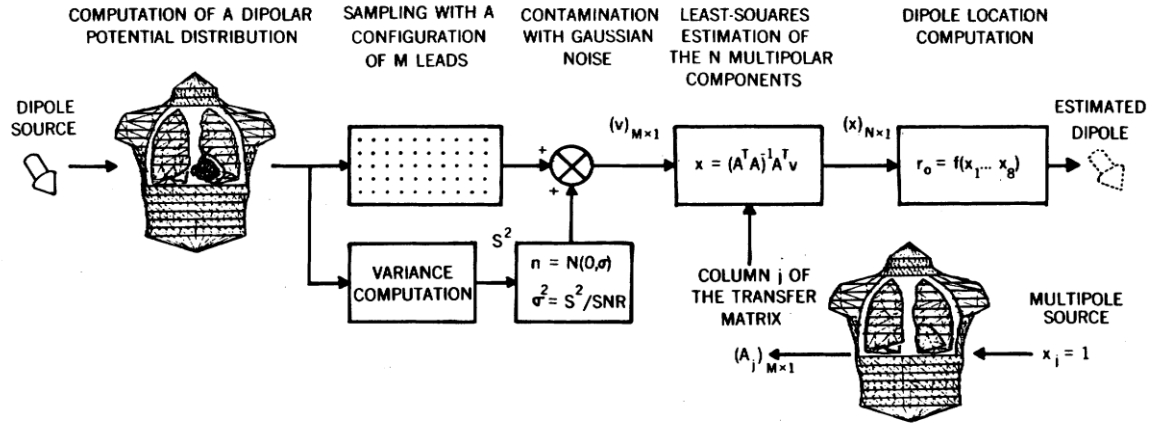

Fig.(10):- Simulation set up of the finite element model of the torso and the block diagram of the mathematical formulation (Savard et al., 1982).

Different lead systems and configuration were used. One by (Lux et al., 1978) which is made of 32 leads another by (Barr et al., 1971) and a third by(Warren, 1978) which consisted of 24 leads and others used up to 192 leads. The main results arrived at by (Savard et al., 1982) concerning the lead number is that although the more the number of electrodes is used the better the single moving dipole (SMD) localization is achieved (Nguyen & Schanze, 2017; Samann et al., 2019) but more than 63 leads electrodes do not give substantial improved results.

Another important factor which also contribute significantly to the accuracy of SMD localization is the electrodes interspacing as the shorter the distance between the electrodes the narrower the field of view which in turn increase the spatial resolution and hence more accurate SMD localization(Goldberger & Ng, 2010).

6. RECENT APPLICATIONS TO MOVING DIPOLE

6-1. Identification of Strict Left Bundle Branch Block

The MVD localization in cardiology can only explain the behavior of normal heart and also can be applied to very localized heart signals as in arrhythmia cases like reentry and left branch bundle block (LBBB); recently the LBBB has gain some attention due to its new definition(Strauss et al., 2011)and also due to the use of cardio resynchronization therapy(CRT) in implantable cardioverter defibrillator(ICD) for the prevention of heart failure and sudden death in arrhythmia diseases(Moss et al., 2009) and in addition, to know who can benefit from CRT. A study by (Bystricky, 2018) in which the ability of how much a MVD representing the heart electrical activity can distinguish between the LBBB new strict definition (hereafter termed sLBBB) and other heart abnormalities was investigated and an automated algorithms were devised to help identify the sLBBB to improve the use of CRT. ECGs published by ISCE initiative 2018 meeting (*LBBB Initiative of the ISCE Meeting.*, 2018) were used, which were 12 lead ECG from male and female having sLBBB taking from Holter device further these were divided into two sets; data set and training set. The definition of the sLBBB by (Strauss et al., 2011) or the complete diagnosis of the sLBBB from the ECG follow the criteria below

1-Duration of QRS complex ≥ 140 ms for male and ≥ 130 ms for female.

2- QS or rS in V1 and V2.

3- Mid-QRS notch in leads I and aVL, slurring in V5 and V6(although slurring can be ignored).

The MVD model used in this study is represented by single time varying signal of momentum q(t) and at position **p**(t). The measured signal was taken at body surface from 8 leads I, II, and the six precordial leads. $m_L(t_i)$ is the measured signal at time t_i ; which represent the scalar product of moment and lead vector L. The lead vector depends on electrode positions, time varying positions, and body geometry and conductivities. The dipole potential Φ(r) (Malmivuo, J., & Plonsey, 1995)] is given by Equation**Error! Reference source not found.**

$$(r) \cong 1/\sigma r^2 \qquad (2)$$

where σ is the conductivity and r the distance from the position of the dipole. The lead vector of electrodes E_j , E_k at position e_j and e_k is given by Equation**Error! Reference source not found.**

$$L_{j,k}(t) = \frac{e_j - p(t)}{\sigma \|e_j - p(t)\|^3} - \frac{e_k - p(t)}{\sigma \|e_k - p(t)\|^3} \qquad (17)$$

Equation**Error! Reference source not found.** can be modified to account for different conductivities related to different electrodes and by small changes in electrode positions from the real position. The predicted lead vector can be calculated as in Equation**Error! Reference source not found.**

$$\hat{m}_{j,k}(t) = L_{j,k}(t) \cdot q(t) \qquad \textbf{Error! Reference source not found.}$$

The estimated equivalent MVD generator is given by minimizing the expression below in Equation**Error! Reference source not found.**

$$\sum_{i=1}^{N} \|m(t_i) - \hat{m}(t_i)\|^2 + \Phi_p(p) + \Phi_q(q) + \Phi_e(e, \tilde{e}) + \Phi_\sigma(\sigma, \tilde{\sigma}) \quad \rightarrow min \qquad \textbf{Error! Reference source not found.}$$

N represents number of sampling points, $\hat{m}(t_i)$ and $m(t_i)$ are predicted and measured vector leads respectively at t_i,and Φ_x (x,x~) represents regularize function related to the prior conditions (model parameter optional values) see (Bystricky, 2012) as shown in Figure11.

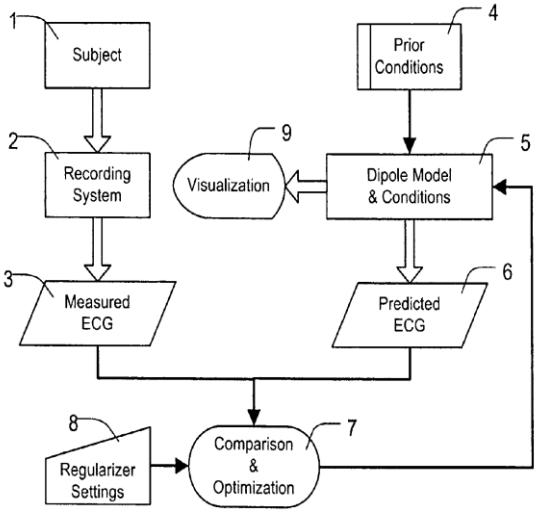

Fig.(11):- Flow diagram identification of the electrical activity in the heart concurrently with subject and measurement related conditions(Bystricky, 2012).

After fitting the MVD to the central five seconds of each ECG a total of 2403 beats were analyzed in five equal time slices starting from 10ms up to 160ms and the position and the momentum of the MVD within the QRS complex were found. These X, Y, and Z of spatial components in addition to QRS width, and sex was applied to a logistic regression(*R Core Team,* 2017) to separate sLBBB and non LBBB cases; an accuracy of 85% were obtained, the MVD model analysis revealed some physiological information too, which are not available in 12 Lead ECG.

6-2. MVD Determination from 12-Lead ECGs and Detection of Acute Myocardial Ischemia

6-2-1. Spatial Distribution and Orientation of a

Single MVD Computed in 12-lead ECGs of a Healthy Population

In a study made by(Starc & Swenne, 2017) relying on the spatial distribution of equivalent source or the single moving equivalent dipole(SMED) localization findings of (Armoundas et al., 2001; Armoundas, Feldman, Mukkamala, & Cohen, 2003) ("source size is largest at the end part of the QRS complex, at depolarization end"); the possibility of assessing the MVD from 12-lead ECG(Bort et al., 2017) in a healthy population for complete cycle was investigated.

By utilizing a model from which a solution to Laplace Equation as in Equation **Error! Reference source not found.** & **Error! Reference source not found.** with the aid of analytical equation of potentials Φ_{ik} Equation**Error! Reference source not found.**, (which represent the scalar product of dipole vector $\overrightarrow{D_k}$ and the lead vector $\overrightarrow{L_{k_i}}$) was obtained; using the method of images for the dipole in homogenous conductive sphere of radius R as shown in Figure12.

$$\Phi_{ik} = \overrightarrow{D_k} \cdot \overrightarrow{L_{k_i}} \tag{20}$$

$$\overrightarrow{L_{k_i}} = \frac{1}{4\sigma\pi R^2} * \left(\frac{\bar{n}'_{ki}}{\left|\overline{\tilde{r}_{ki}}/_R\right|^2} + \frac{\overline{\tilde{n}_{ki}} - 2\left(\overline{n'_k} \cdot \overline{\tilde{n}_{ki}}\right)\overline{n'_k}}{f^3 \left|\overline{\tilde{r}_{ki}}/_R\right|^2} + h \right) \tag{21}$$

$$h = -\frac{\bar{n}_{kt}}{f}\frac{\bar{n}_k}{f} + \frac{\left(\mu + (f-\mu)/\sqrt{(1+f^2-2fu)}\right)}{\sqrt{(1-u^2)}} \tag{22}$$

$\overrightarrow{D_k}$ and $\overrightarrow{D'_k}$, σ are dipole and its mirroring image, the conductivity of the medium respectively, , $\mu, f,$ are as indicated in the diagram of Figure12 and **h** is the potential part to make the solution consistent with Laplace solution for surface potential

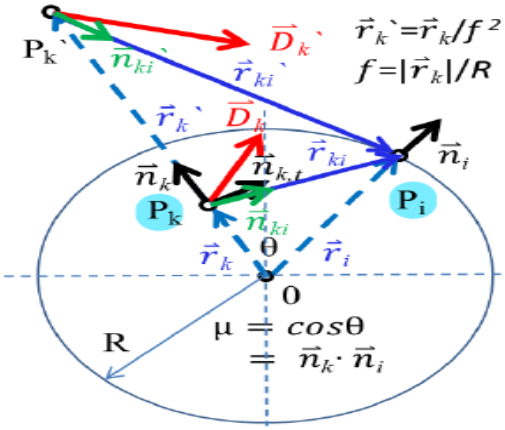

Fig.(12):- Representation MVD model, in the plane through the points Pk , Pi, and the sphere origin. The dipole and its image are both in red (Starc & Swenne, 2017).

A human torso model was constructed using data from(Dawoud et al., 2008) which also included the location of electrodes for the ECG, the model was a sphere of radius 15 cm and the potentials of the ECG electrode(the measured potentials V_{ik}) were 9; six precordial and the VR, VL, and VF all taken with the reference to Wilson terminal. Dipole strength and direction was obtained by minimizing the Equation**Error! Reference source not found.** after substituting Equation**Error! Reference source not found.** into Equation**Error! Reference source not found.**

$$F_{ik} = \Phi_{ik} - V_{ik} \quad (23)$$

$$F_{ik} = \overrightarrow{D_k} . \overrightarrow{L_{kı}} - V_{ik} \quad (24)$$

Where F_{ik} the error function. The values of D_{kx}, D_{ky}, and D_{kz} were obtained by using principal component analysis. This solution gave the direction and the strength, to get the location an objective function $\psi(r_k)$ Equation**Error! Reference source not found.** was minimized and also normalized by the sum of potentials squared. For further detailed see(Starc & Swenne, 2017).

$$\psi(\bar{r_k}) = \sum_{i=1}^{Ni} F_{ik}^2 / \sum_{i=1}^{Ni} V_{ik}^2 \quad (25)$$

The range of movement of MVDs in three dimensions (MVD ROM) was defined as relative deviation of the mean from the average of the MVD location during QT interval. 16-segment model was employed in a single ECG beat of each subject to obtain the spatial distribution of MVDs in a healthy population; QRS was represented by 10 segments, the remaining 6 segments were used; 3 segments for each of ST and T wave respectively. These segment representations were averaged over each single beat(for averaging details see(Starc & Swenne, 2017)) and further over the whole 20 beats which were chosen for this template.

The location and the orientation of this spatial distribution were quantified in 1.5 cm^3 voxels. The mean MVD orientation and the intra voxel dispersion were also obtained for each voxel. The main finding of this study was that for the healthy population considered the MVD spatial distribution at similar time instants are over small volume and with small intra voxel dispersion, which permit the use of ECG segment representation of the MVD spatial distribution orientations and locations as a reference to compare with and identify abnormalities as in cardiac ischemia or infarction that have dissimilar distributions.

6-2-2. MVD Determination from12 Lead ECGs and Ischemia Detection

Using the findings above (Starc & Swenne, 2017) and ECG data from STAFF III data base (Martínez et al., 2017) which are related to patients who suffered occlusion in right coronary artery RCA or left circumflex LCX or left descending artery LDA an investigating study by(Starc & Schlegel, 2020) was conducted and under the assumption that depolarization changes in ischemia lead to changes in SMEDs locations which in turn might help in discovering its position and detecting it; something difficult to detect in 12 lead ECG specially in RDA and LCX. The heart model employed was that of 12cm sphere positioned in the left anterior part of the chest using data from (Odille et al., 2017) as shown Figure13, to fit all the hearts in the data base an assumption was made that all follow the heart orientation in the MRI study(Odille et al., 2017) combining those data a heart model was formed with ellipsoidal right ventricle(RV) and left ventricle(LV) further the long axis was aligned with LV and short axis perpendicular to the septum center. The SMED trajectory was assumed to coincide with the origin of LV at the beginning of the QRS.

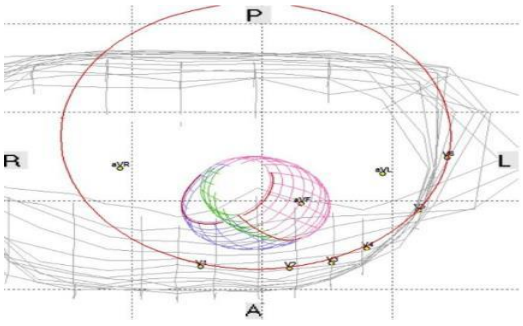

Fig.(13):- Heart location in the chest (Starc & Schlegel, 2020).

To represent the SMED in heart in local coordinates a 12 segment LV model was

identified with the arteries supply as shown in Figure14 and 15(Selvester et al., 2010).

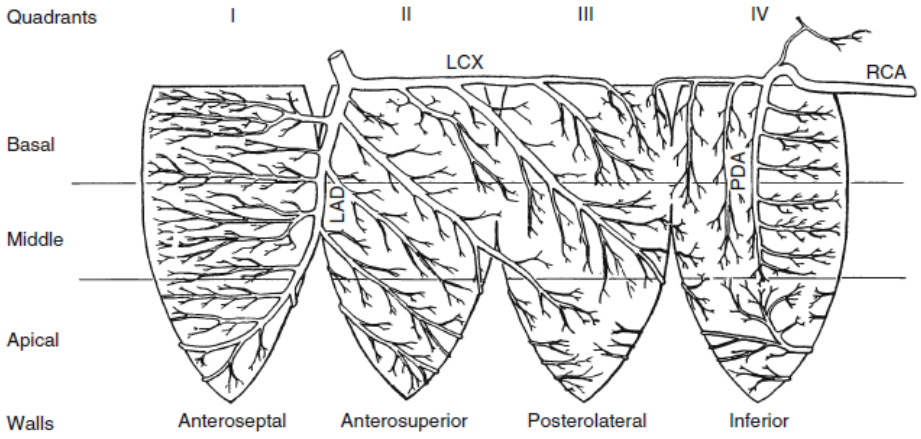

Fig.(14):- Typical distribution of heart coronary arteries on epicardial surface. The superior 75-80 % of the anteroseptal wall is supplied by septal perforator branches of (LAD). The remaining 20-25% of the inferior parts is supplied by the shorter septal branches of the posterior (inferior) descending artery (PDA) (Selvester et al., 2010).

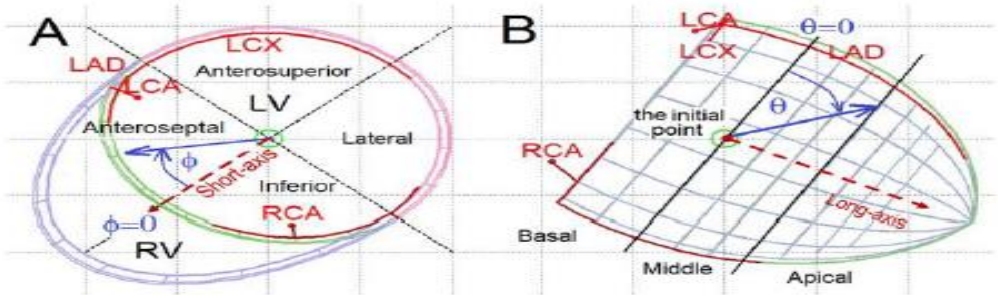

Fig.(15):- A: Short axis view wall segments, and B: long axis view, the coronary arteries(Starc & Schlegel, 2020).

The location of SMEDs in a healthy population was restricted within small volume and orientation limited in the intraventricular plane (Starc & Swenne, 2017) and their projections on short axis for the QRST and on the long axis the at the end portion of T wave; shown in Figure16, A and B respectively.

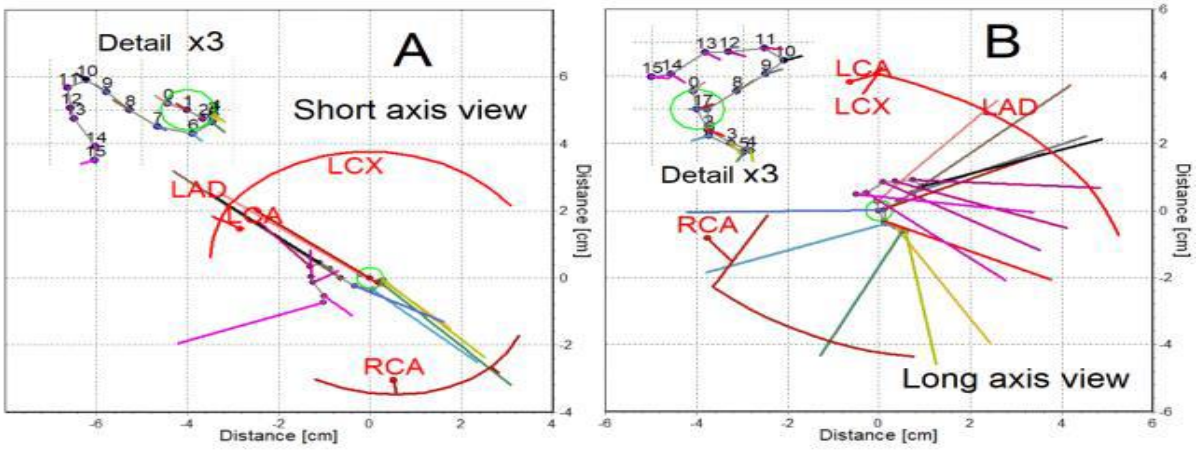

Fig.(16):- The changing aspects of SMEDs in a healthy population, A: short axis view, B: long axis view. Color coding: QRS0-QRS9, from the initial light red changing via yellow, green, and blue to gray; ST1-ST3, black; T1-T3, violet; Each SMED represents the mean value of 563 individuals (Starc & Schlegel, 2020).

The behavior of SMEDs in the occluded LCX and RCA arteries differ noticeably from healthy population behavior in that it showed dipolar amplitude increase, location change of SMEDs of the QRS and ST segments from initial to inferior or posterior wall depending on the unhealthy artery, and directed toward the affected wall segment then returning to the former orientation next to recovery. The SMED in rest (green) against occluded (red) are easy recognizable Figure17

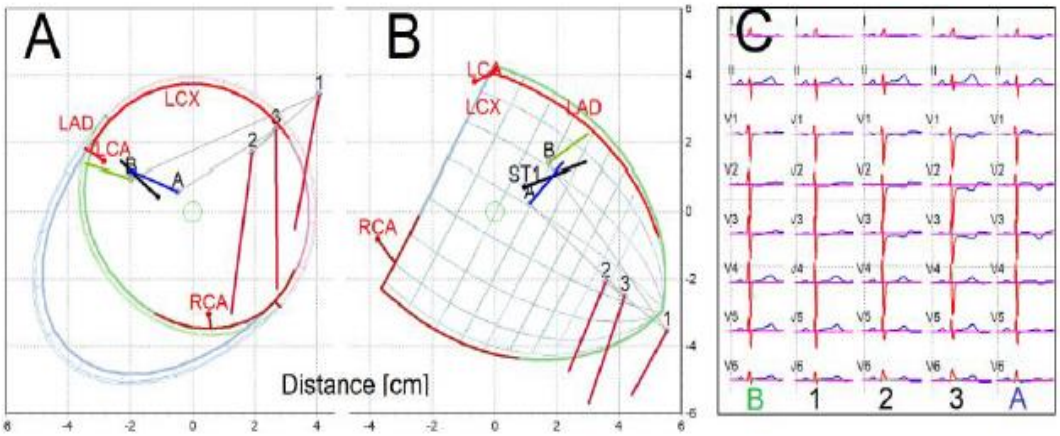

Fig.(7):- The properties of SEMDs variation in the ST segment within the LCX artery proximal occlusion in different intervention phases. The phases of C: 12 lead ECG are as follow: B stands for before occlusion(green), A stands for after occlusion (blue), and 1,2 and 3 during occlusion for 1,3, and 5 minutes in red respectively. The SMEDs of the ST1 group in black(Starc & Schlegel, 2020)

In the occlusion of the LAD artery the ST segment showed increase dipolar amplitude but the SMED s orientation were not considerable; may be because of overlapping with ST segment Figure17C.

Table(1):- Segments of ECG cycle and projection on different heart part. Azimuth dynamic of the heart in QRS end and ST segment

Group	N	Q6	Q7	Q8	Q9	ST1	ST2
Control	511	**-62**	**-4**	82	91	98	101
prox.RCA	42	**-69**	**-54**	**-5**	22	24	52
mid.RCA	33	**-76**	**-36**	**-16**	33	42	37
dist.RCA	24	**-73**	**-60**	**-34**	**-15**	**-8**	46
prox.LCX	24	**-84**	**-75**	**-57**	5	12	11
mid.LCX	12	**-91**	**-61**	**-27**	**-4**	**-8**	**-15**
dist.LCX	16	**-80**	**-69**	**-59**	**-42**	**-40**	**-34**
prox.LDA	56	**-67**	97	101	96	96	98
mid.LDA	25	**-59**	-26	85	89	91	98

The findings of this study are that the most changes of the SMEDs amplitude location and orientation during occlusion in the RCA and LCX arteries that are difficult to be detected in 12 lead ECG manifest itself very early with low ST segment, and they are not just on the ST segment but also on the end portion of QRS. In spite of inconsistency in the change of pattern of the SMEDs this method can help in detection of ischemia of the inferior wall of the occlusion in RCA and LCX.

7. CONCLUSIONS

SMD is proven theoretically, experimentally, and clinically to be responsible for more than 99.3% of the total electric field appearing on surface method (non- invasive); whether body surface or epicardial (even more in the case of invasive in the endocardial method), and in volume method where the body is divided into small elements using the finite element method. The practical localization method (in the presence of noise) by the inverse method although non unique and very susceptible to noise level and geometry, both of body and electrodes, it could be improved by using a larger number of electrodes up to certain limit depending on the geometry beyond which no appreciable improvement can be obtained. The localization of the SMD can be further improved by shortening the interelectrode spacing as this distance can improve the field of

view of the lead system and a better spatial resolution(localization) can be obtained.

Interesting trends of applications are recently appearing for the MVD that help in detection of isolated ectopic signals of arrythmia in implantable cardioverter defibrillator(ICD) devices that can deliver CRT and also identify how need them, like in cases of sLBBB. Furthermore, MVD can contribute greatly in reviving the role of 12 lead ECG as diagnostic tool again by ECG MRI projection pattern that will lead to the early detection and identification of ischemia in RCA and LCX that were difficult to detect by 12 lead ECG. The benefit of this early detection by this 12 lead ECG manifests itself in

1. The prevention of wrong drug administrating(nitroglycerine) to patients having ischemia/infarction symptoms which may lead to fatal errors (hemodynamic collapse) in RCA occlusion cases.

2. I very important in pinpointing the clipart artery which in turn greatly reduce the time for catheterization procedure as it helps the interventional cardiologists in choosing the right catheter.

3. The ease of use, fast results, and unexpansive of 12 lead ECG as it's a well-established tool for all medical staff compared to other modalities like Echocardiography and MRI greatly reduces inpatient time.

Future work should include the enhancement in acquisition and mathematical processing of the low ST segment signal as it's very important in localizing the SMD and this may be achieved by proper electrode placement and change in electrode size.

REFERENCES

Armoundas, A. A., Feldman, A. B., Mukkamala, R., & Cohen, R. J. (2003). A single equivalent moving dipole model: An efficient approach for localizing sites of origin of ventricular electrical activation. *Annals of Biomedical Engineering*, *31*(5), 564–576. https://doi.org/10.1114/1.1567281

Armoundas, A. A., Feldman, A. B., Mukkamala, R., He, B., Mullen, T. J., Belk, P. A., Lee, Y. Z., & Cohen, R. J. (2003). Statistical Accuracy of a Moving Equivalent Dipole Method to Identify Sites of Origin of Cardiac Electrical Activation. *IEEE Transactions on Biomedical Engineering*, *50*(12), 1360–1370. https://doi.org/10.1109/TBME.2003.819849

Armoundas, A. A., Feldman, A. B., Sherman, D. A., & Cohen, R. J. (2001). Applicability of the single equivalent point dipole model to represent a spatially distributed bio-electrical source. *Medical and Biological Engineering and Computing*, *39*(5), 562–570. https://doi.org/10.1007/BF02345147

Barnard, A. C. L., Duck, I. M., Lynn, M. S., & Timlake, W. P. (1967). The Application of Electromagnetic Theory to Electrocardiology: II. Numerical Solution of the Integral Equations. *Biophysical Journal*, *7*(5), 463–491. https://doi.org/10.1016/S0006-3495(67)86599-8

Barr, R. C., Spach, M. S., & Herman-giddens, G. S. (1971). Measuring Locations. *IEEE Transactions on Biomedical Engineering*, *BME-18*(2), 125–138.

Bort, R., Mascarell, L., Rodrigo, M., Climent, A. M., Liberos, A., Hernández-romero, I., Arenal, A., Bermejo, J., Fernández-avilés, F., Atienza, F., & Guillem, M. S. (2017). *This paper must be cited as : Solving inaccuracies in anatomical models for electrocardiographic inverse problem resolution by using electrical information*. *37*(3), 733–740.

Brody, D. A., Warr, O. S., Wennemark, J. R., Cox, J. W., Keller, F. W., & Terry, F. H. (1971). Studies of the equivalent cardiac generator behavior of isolated turtle hearts. *Circulation Research*, *29*(5), 512–524. https://doi.org/10.1161/01.RES.29.5.512

Brody, D. A., & Wennemark, J. R. (1974). Dipole ranging in isolated rabbit hearts before and after right bundle branch block'. In *Cardiovascular Research* (Vol. 8).

Bystricky, W. (2012). *MODELING THE ELECTRICAL ACTIVITY OF THE HEART BY A SINGLE DIPOLE, CONCURRENTLY ESTMLATING SUBJECT AND MEASUREMENT RELATED CONDITIONS*.

Bystricky, W. (2018). Identification of Strict Left Bundle Branch Block, Using a Moving Dipole Model. *Computing in Cardiology*, *2018-Septe*. https://doi.org/10.22489/CinC.2018.216

Claydon, F. J., Milligan, K. L., Gray, T. E., & Mirvis, D. M. (1992). An equivalent generator representation of measured intracavitary potentials. *Proceedings of the Annual International Conference of the IEEE Engineering in Medicine and Biology Society, EMBS*, *2*, 582–583. https://doi.org/10.1109/IEMBS.1992.5761120

Dawoud, F., Wagner, G. S., Moody, G., & Horáček, B. M. (2008). Using inverse electrocardiography to image myocardial infarction-reflecting on the 2007 PhysioNet/Computers in Cardiology Challenge. *Journal of Electrocardiology*, *41*(6), 630–635. https://doi.org/10.1016/j.jelectrocard.2008.07.022

Gabor, D., & Nelson, C. V. (1954). Determination of the resultant dipole of the heart from measurements on the body surface. *Journal of Applied Physics*, *25*(4), 413–416. https://doi.org/10.1063/1.1721655

Geselowitz, D. B. (1964). Dipole theory in

electrocardiography. *The American Journal of Cardiology*, *14*(3), 301–306. https://doi.org/10.1016/0002-9149(64)90072-4

Geselowitz, D. B. (1965). Two Theorems Concerning the Quadrupole Applicable to Electrocardiography. *IEEE Transactions on Biomedical Engineering*, *BME-12*(3), 164–168. https://doi.org/10.1109/TBME.1965.4502373

Goldberger, J. J., & Ng, J. (2010). Practical signal and image processing in clinical cardiology. In *Practical Signal and Image Processing in Clinical Cardiology*. https://doi.org/10.1007/978-1-84882-515-4

Gulrajani, R. M. (1998). The forward and inverse problems of electrocardiography: Gaining a better qualitative and quantitative understanding of the heart's electrical activity. *IEEE Engineering in Medicine and Biology Magazine*, *17*(5). https://doi.org/10.1109/51.715491

Horáček, B. M. (1971). *The Effect on Electrocardiographic Lead Vectors of Conductivity Inhomogeneities in the Human Torso*. Dalhousie University.

Horan, L. G., Flowers, N. C., & Miller, C. B. (1972). A rapid assay of dipolar and extradipolar content in the human electrocardiogram. *Journal of Electrocardiology*, *5*(3), 211–223. https://doi.org/10.1016/S0022-0736(72)80001-3

Houari, K. El, Kachenoura, A., Albera, L., Bensaid, S., Karfoul, A., Boichon-Grivot, C., Rochette, M., & Hernández, A. (2018). A fast model for solving the ECG forward problem based on an evolutionary algorithm. *2017 IEEE 7th International Workshop on Computational Advances in Multi-Sensor Adaptive Processing, CAMSAP 2017*, *2017-December*(June 2018), 1–5. https://doi.org/10.1109/CAMSAP.2017.8313083

Ideker, R. E., Bandura, J. P., Larsen, R. A., Cox, J. W., Keller, F. W., & Brody, D. A. (1975). *Localization of Heart Vectors Produced by Epicardial Burns and Ectopic Stimuli VALIDATION OF A DIPOLE RANGING METHOD*. http://ahajournals.org

Kabanikhin, S. I. (2008). Definitions and examples of inverse and ill-posed problems Survey paper. *J. Inv. Ill-Posed Problems*, *16*, 317–357. https://doi.org/10.1515/JIIP.2008.069

Kay, C. F. Schwan, H. P. (1956). Specific resistance of body tissues. *Circulation Research*, *4*(6), 664–670. https://doi.org/10.1161/01.res.4.6.664

LBBB Initiative of the ISCE meeting. (2018). http://www.thew-project.org/LBBB_Initiative.htm

Lux, R. L., Smith, C. R., Wyatt, R. F., & Abildskov, J. A. (1978). Limited Lead Selection for Estimation of Body Surface Potential Maps in Electrocardiography. *IEEE Transactions on Biomedical Engineering*, *BME-25*(3), 270–276. https://doi.org/10.1109/TBME.1978.326332

Lv, W., Lee, K., Arai, T., Barrett, C. D., Hasan, M. M., Hayward, A. M., Marini, R. P., Barley, M. E., Galea, A., Hirschman, G., Armoundas, A. A., & Cohen, R. J. (2020). Accuracy of cardiac ablation catheter guidance by means of a single equivalent moving dipole inverse algorithm to identify sites of origin of cardiac electrical activation. In *Journal of Interventional Cardiac Electrophysiology* (Vol. 58, Issue 3). https://doi.org/10.1007/s10840-019-00605-z

Lynn, M. S., & Timlake, W. P. (1968). The Use of Multiple Deflations in the Numerical Solution of Singular Systems of Equations, with Applications to Potential Theory. *SIAM Journal on Numerical Analysis*, *5*(2), 303–322. https://doi.org/10.1137/0705027

Macfarlane, P. W., Van Oosterom, A., Pahlm, O., Kligfield, P., Janse, M., & Camm, J. (2010). *Comprehensive electrocardiology.* (Second Edi). Springer Science & Business Media. https://doi.org/10.1007/978-1-84882-046-3

Malmivuo, J., & Plonsey, R. (1995). *Bioelectromagnetism: principles and applications of bioelectric and biomagnetic fields.* Oxford University Press. https://doi.org/10.1093/acprof:oso/9780195058239.001.0001

Martin Arthur's, R., Geselowitz, D. B., Briller, S. A., & Trost, R. F. (1971). The Path of the Electrical Center of the Human Heart Determined from Surface Electrocardiograms*. In *J. ELECTROCARDIOLOGY* (Vol. 4, Issue 1).

Martínez, J. P., Pahlm, O., Ringborn, M., Warren, S., Laguna, P., & Sörnmo, L. (2017). The STAFF III Database: ECGs recorded during acutely induced myocardial ischemia. *Computing in Cardiology*, *44*(September), 1–4. https://doi.org/10.22489/CinC.2017.266-133

McFee, R., & Baule, G. M. (2008). Research in electrocardiography and magnetocardiography. *Proceedings of the IEEE*, *60*(3), 290–321. https://doi.org/10.1109/proc.1972.8621

Moss, A. J., Hall, W. J., Cannom, D. S., Klein, H., Brown, M. W., Daubert, J. P., Estes, N. A. M., Foster, E., Greenberg, H., Higgins, S. L., Pfeffer, M. A., Solomon, S. D., Wilber, D., & Zareba, W. (2009). Cardiac-Resynchronization Therapy for the Prevention of Heart-Failure Events. *New England Journal of Medicine*, *361*(14), 1329–1338. https://doi.org/10.1056/nejmoa0906431

Nakane, T., Ito, T., Matsuura, N., Togo, H., & Hirata, A. (2019). Forward electrocardiogram modeling by small dipoles based on whole-body electric field analysis. *IEEE Access*, *7*, 123463–123472. https://doi.org/10.1109/ACCESS.2019.2938409

Nakano, Y., Rashed, E. A., Nakane, T., Laakso, I., & Hirata, A. (2021). Ecg localization method based on volume conductor model and kalman

filtering. *Sensors*, *21*(13). https://doi.org/10.3390/s21134275

Nelson, C. V., Gastonguay, P. R., Wilkinson, A. F., & Voukydis, P. C. (1971). A lead system for direction and magnitude of the heart vector. *Vectorcardiography*, *2*, 85–97.

Nelson, C. V., Rand, P. W., Angelakos, E. T., & Hugenholtz, P. G. (1972). Effect of intracardiac blood on the spatial vectorcardiogram. I. Results in the dog. In *Circulation research* (Vol. 31, Issue 1). https://doi.org/10.1161/01.RES.31.1.95

Nelson, C. V, Hodgkin, B. C., & Voukydis, P. C. (1975). Determination of the Locus of the Heart Vector from Body Surface Measurements: Model Experiments. In *J. ELECTROCARDIOLOGY* (Vol. 8, Issue 2).

Nguyen, M., & Schanze, T. (2017). Spatial resolution of electrical source localization depends on inter-electrode spacing and signal-to-noise ratio. *Current Directions in Biomedical Engineering*, *3*(2), 87–90. https://doi.org/10.1515/cdbme-2017-0019

Odille, F., Liu, S., Van Dam, P., & Felblinger, J. (2017). Statistical variations of heart orientation in healthy adults. *Computing in Cardiology*, *44*, 1–4. https://doi.org/10.22489/CinC.2017.225-058

Plonsey, R., & Barr, R. C. (2007). *Bioelectricity A Quantitative Approach* (Third Edit). Springer Science & Business Media. https://doi.org/10.1007/978-0-387-48865-3

R Core Team,. (2017). https://www.r-project.org/R System

Rush, S. (1971). An inhomogeneous anisotropic model of the human torso for electrocardiographic studies. *Medical and Biological Engineering*, *9*, 201–211.

Samann, F., Rausch, A., & Schanze, T. (2019). Electrical Dipole Source Localization using Hybrid Least Squares Method in combination with ICA. *Current Directions in Biomedical Engineering*, *5*(1), 361–363. https://doi.org/10.1515/cdbme-2019-0091

Savard, P., Ackaoui, A., Gulrajani, R. M., Nadeau, R. A., Roberge, F. A., Guardo, R., & Dube, B. (1985). Localization of cardiac ectopic activity in man by a single moving dipole. Comparison f different computation techniques. In *Journal of Electrocardiology* (Vol. 18, Issue 3). https://doi.org/10.1016/S0022-0736(85)80045-5

Savard, P., Mailloux, G. E., Roberge, F. A., Gulrajani, R. M., & Guardo, R. (1982). A Simulation Study of the Single Moving Dipole Representation of Cardiac Electrical Activity. *IEEE Transactions on Biomedical Engineering*, *BME-29*(10), 700–707. https://doi.org/10.1109/TBME.1982.324863

Selvester, R. H., Strauss, D. G., & Wagner, G. S. (2010). *Myocardial Infarction BT - Comprehensive Electrocardiology*. Springer Verlag. https://doi.org/10.1007/978-1-84882-046-3_16

Starc, V., & Schlegel, T. T. (2020). Moving Dipole Determination from 12-Lead ECGs Can Improve Detection of Acute Myocardial Ischemia. *Computing in Cardiology*, *2020-September*. https://doi.org/10.22489/CinC.2020.115

Starc, V., & Swenne, C. A. (2017). Spatial distribution and orientation of a single moving dipole computed in 12-lead ECGs of a healthy population using a spherically bounded model. *Computing in Cardiology*, *44*, 1–4. https://doi.org/10.22489/CinC.2017.242-277

Strauss, D. G., Selvester, R. H., & Wagner, G. S. (2011). Defining left bundle branch block in the era of cardiac resynchronization therapy. In *American Journal of Cardiology* (Vol. 107, Issue 6, pp. 927–934). https://doi.org/10.1016/j.amjcard.2010.11.010

Svehlikova, J., Teplan, M., & Tysler, M. (2018). Geometrical constraint of sources in noninvasive localization of premature ventricular contractions. *Journal of Electrocardiology*, *51*(3), 370–377. https://doi.org/10.1016/j.jelectrocard.2018.02.013

Taccardi, B., Arisi, G., Macchi, E., Baruffi, S., & Spaggiari, S. (1987). A new intracavitary probe for detecting the site of origin of ectopic ventricular beats during one cardiac cycle. *Circulation*, *75*(1), 272–281. https://doi.org/10.1161/01.CIR.75.1.272

Terry, F. H., Brody, D. A., Cox, J. W., Keller, F. W., & Phillips, H. A. (1971). Dipole, Quadripole, and Octapole Measurements in Isolated Beating Heart Preparations. In *IEEE TRANSACTONS ON BIO-MEDICAL ENGINEERING* (Vol. 18, Issue 2).

Warren, R. B. (1978). *DETERMINING THE NUMBER AND POSITIONS OF MEASURING LOCATIONS FOR BODY SURFACE POTENTIAL MAPPING*.